HHS Public Access

Author manuscript

Nat Chem Biol. Author manuscript; available in PMC 2017 January 11.

Published in final edited form as:

Nat Chem Biol. 2016 September ; 12(9): 709–716. doi:10.1038/nchembio.2126.

Conformationally Selective RNA Aptamers Allosterically Modulate the β_2-Adrenoceptor

Alem W. Kahsai[1], **James W. Wisler**[1], **Jungmin Lee**[1,7], **Seungkirl Ahn**[1], **Thomas J. Cahill III**[1,2], **S. Moses Dennison**[5], **Dean P. Staus**[1], **Alex R. B. Thomsen**[1], **Kara M. Anasti**[5], **Biswaranjan Pani**[1], **Laura M. Wingler**[1], **Hemant Desai**[9], **Kristin M. Bompiani**[3,4,11], **Ryan T. Strachan**[8], **Xiaoxia Qin**[10], **S. Munir Alam**[5], **Bruce A. Sullenger**[3,4], and **Robert J. Lefkowitz**[1,2,6,*]

[1]Department of Medicine, Duke University Medical Center, Durham, NC, 27710

[2]Department of Biochemistry, Duke University Medical Center, Durham, NC, 27710

[3]Department of Surgery, Duke University Medical Center, Durham, NC, 27710

[4]Duke Translational Research Institute, Duke University Medical Center, Durham, NC, 27710

[5]Duke Human Vaccine Institute, Duke University Medical Center, Durham, NC, 27710

[6]Howard Hughes Medical Institute, Duke University Medical Center, Durham, NC, 27710

[7]Department of Chemistry and Chemical Biology, Harvard University, Cambridge, MA 02138

[8]Department of Pharmacology, Chapel Hill, NC 27516

[9]The University of North Carolina School of Medicine, Chapel Hill, NC 27516

[10]Genome Sequencing and Analysis Core Resource, Duke University, Durham, NC, 27710

[11]The University of California, San Diego, Moores Cancer Center, La Jolla, CA 92093

Abstract

G-protein-coupled receptor (GPCR) ligands function by stabilizing multiple, functionally distinct receptor conformations. This property underlies how “biased agonists” activate specific subsets of a given receptor’s signaling profile. However, stabilization of distinct active GPCR conformations to enable structural characterization of mechanisms underlying GPCR activation remains difficult.

*Correspondence and requests for materials should be addressed to R.J.L. (lefko001@receptor-biol.duke.edu).

Author contributions

A.W.K., J.W.W., S.A., B.A.S., and R.J.L. conceived the study. A.W.K, J.W.W, K.M.P, and H.D. performed selection, and enrichment analysis. A.W.K, J.W.W., L.M.W., B.A.S., and R.J.L. designed NGS strategies. A.W.K., J.L., and H.D. performed Illumina-NGS library construction, preparations, and quality control analysis. A.W.K., J.L., H.D., X.Q., and L.M.W. participated in writing custom scripts and NGS data analysis. A.W.K, and J.L. performed aptamer synthesis, biotinylation, and fluorescent studies. S.M.D., K.M.A., and S.M.A. conducted BLI experiments. A.W.K., J.W.W., J.L., D.P.S., B.P., A.R.B.T., H.D., and R.T.S. participated in binding studies, receptor functionality tests, and reconstitution in HDL particles. S.A. conducted functional experiments. T.J.C. and A.R.B.T with assistance from A.W.K. and J.L. performed EM imaging and particle analysis. A.W.K., B.A.S., and R.J.L. wrote the manuscript. All authors contributed in preparing and editing of the manuscript.

Competing financial interests

The authors declare no competing financial interests.

These challenges have accentuated the need for receptor tools that allosterically stabilize and regulate receptor function via unique, previously unappreciated mechanisms. Here, utilizing a highly diverse RNA library combined with advanced selection strategies involving state-of-the-art next-generation sequencing and bioinformatics analyses, we identify RNA aptamers that bind a prototypical GPCR, β_2-adrenoceptor (β_2AR). Using biochemical, pharmacological, and biophysical approaches, we demonstrate that these aptamers bind with nanomolar affinity at defined surfaces of the receptor, allosterically stabilizing active, inactive, and ligand-specific receptor conformations. The discovery of RNA aptamers as allosteric GPCR modulators significantly expands the diversity of ligands available to study the structural and functional regulation of GPCRs.

INTRODUCTION

G protein–coupled receptors (GPCRs) are the superfamily of cell-surface, seven α-helical transmembrane-spanning receptors, with over 800 members identified in the human genome[1–4]. GPCRs are targets of one-third of all pharmaceutical agents currently available on the market for treatment of a wide range of health problems including cardiovascular disease, neurological disorders, asthma, and immune system dysfunction[1,3]. In response to agonist binding, GPCRs undergo conformational changes that activate intracellular signaling cascades and effector systems via coupling to G proteins and G protein–independent transducers such as β-arrestins[2,5,6]. Importantly, these two signaling pathways can be pharmacologically separated through the use of “biased” agonists that preferentially activate one signaling arm over the other, potentially leading to therapeutics with more targeted efficacy and enhanced safety profiles[5–8]. Indeed, work over the past decade has led to a list of biased agonists for several GPCRs and some of these biased agonists have even entered late stage clinical trials for various disease conditions[6–8].

The development of such biased ligands is dependent on a detailed understanding of the structural basis of different signaling GPCR conformations. Numerous biophysical studies have demonstrated that GPCRs are dynamic allosteric machines that exhibit conformational heterogeneity in both ligand-occupied and ligand-free states[9–11]. These studies support a multi-state model for GPCR activation in which receptors adopt multiple active or inactive conformations and specific ligands have a propensity to stabilize distinct conformational states and elicit ligand-specific activity. Therefore, structural information is essential to improve our understanding of the nature of ligand-specific receptor conformations and the mechanism by which these allosteric conformational changes are transmitted to transducers to initiate downstream signaling. Although recent crystal structures of multiple GPCRs have provided significant atomic-level structural information[12–16], major challenges still exist in using X-ray crystallography to study the structures of GPCRs. These challenges stem primarily from the inherent flexibility and biochemical instability of functionally active conformational states[9,11,15,17]. X-ray crystallography of GPCRs in the absence of stabilizing agents tends to capture lower energy, thermodynamically stable inactive structures even in the presence of high-affinity or covalently tethered agonists of orthosteric site, thus missing functionally active signaling conformations[11,17,18].

Expanding the chemical profile of GPCR ligands has the potential both to aid in the development of biased drugs for various therapeutically important GPCRs and to provide molecular tools for structural and biophysical applications. Given their molecular diversity, ability to adopt unique 3D structures, lack of immunogenicity, and ease of chemical-modification, RNA aptamers are emerging as valuable pharmacologic agents and conformation-sensors for various targets[19–32]. While aptamers targeting a variety of molecules ranging from small molecules to whole cells have been identified, few studies have described the selection of RNA aptamers against membrane proteins such as GPCRs[20,24–27]. Additionally, most of these studies utilized traditional selection strategies, specifically, using complex cellular systems as targets and characterizing the most abundant aptamers after selection using conventional cloning methods. We hypothesized that isolating RNA aptamers with defined conformational specificities for GPCRs would require precise control of the selection conditions and more sensitive methods for analyzing clones. Here, we describe an integrated approach to discover conformationally specific RNA aptamer allosteric modulators for the β_2-adrenoceptor (β_2AR)[2], a model GPCR system, involving next-generation sequencing (NGS)[33,34] and comparative bioinformatics analysis of parallel selections against purified β2AR in different states. The resulting set of aptamers exhibit distinct preferences for binding to various β_2AR conformational states with high affinity and selectivity, as determined using a combination of biochemical, functional, biophysical and structural methods. Thus, our study reveals the potential of RNA aptamers to serve as molecular tools for elucidating the structural and mechanistic details underlying GPCR activation as well as for developing improved therapeutics.

RESULTS

Preparation of the β_2AR target

The β_2AR is a prototypic and well-characterized member of the GPCR family. It was the first ligand binding GPCR to be cloned and its structure was solved at high resolution in the active state and in complex with G-protein[2,12,13,16]. Purification of functionally active receptor and stabilization of purified GPCRs are major challenges in the field of GPCR biology research. We prepared β_2AR from baculovirus-mediated expression in *Spodoptera frugiperda* (Sf9) insect cells via solubilization in detergent and using a three-step affinity purification procedure (as previously described[4]; see online **Methods**). Purification of the β_2AR to homogeneity was achieved primarily by use of the alprenolol affinity purification step, which selectively isolates functional receptors from those that are non-functional and incapable of binding of radioligand[2,4]. We maintained the purified receptor in maltose–neopentyl glycol (MNG)[35], an amphiphilic detergent that enhances receptor stability. In order to lock the receptor into an active conformation for selection of RNA aptamers, an agonist of high affinity and extremely slow off-rate, BI167107[12,36], was used (Fig. 1a).

Enrichment of conformationally specific RNA aptamers

To develop a strategy that would allow us to identify high affinity, conformationally specific RNA aptamers that recognize β_2AR, we used a highly diverse, 2′-fluoropyrimidine modified, nuclease-resistant RNA library containing approximately 10^{15} unique sequences. Our approach combines an iterative *in vitro* selection process with NGS technology and

comparative bioinformatics analysis to efficiently identify candidate aptamer binders with desired functional properties (Fig. 1a and see Supplementary Results, Supplementary Fig. 1 for a detailed selection schematics)[31–34]. To isolate unique RNA aptamers that bind at structurally relevant sites on the β_2AR, we performed nine rounds of positive selection against unliganded-β_2AR and a high-affinity agonist (BI167107)-bound β_2AR. Prior to each round of positive selection, we performed negative selection to deplete filter and other non-target-binding RNA molecules. In order to further enrich the population for aptamers that bound to our targets, at round five we performed a counter-selection against a non-target membrane protein, an inactive angiotensin receptor subtype 1a (AT1aR). Enrichment of target-specific sequences was monitored by measuring bulk equilibrium dissociation constants (K_d) of successive aptamer pools for binding to the two β_2AR selection targets, via a nitrocellulose filter binding assay (Supplementary Fig. 2). We found that the initial library, and pools from R1 through R4 exhibited minimal binding, but we observed a noticeable increase in the binding affinity of the R5 pool for each selection target (β_2AR and β_2AR:BI167107). Accordingly, all selected RNA pools starting from R5 on exhibited a progressive increase in the binding affinity, with the most prominent enrichments occurring between rounds 6 and 9 (Supplementary Fig. 2). For example, aptamer pools from round 9 displayed nanomolar binding affinities for both selection targets (K_d [R9 pool binding to unliganded β_2AR] = 99.4 ± 15.6 nM and K_d [R9 pool binding to β_2AR: BI167107] = 86.2 ± 11.2 nM).

NGS of the eluted aptamer pools improved the resolution of the data over that of traditional single clone Sanger sequencing method. Traditional sequencing method limits sampling to a potentially poorly representative portion of the clonal space (usually a few hundred clones) compared to NGS, which samples millions of sequences across successive rounds of selection. The ability to sample a large proportion of clonal space via NGS not only improves the power of the selection, but also reduces the risk of capturing non-specific or poorly representative clones. High-throughput sequencing (HTS) was accomplished by preparing multiple barcoded, Illumina-compatible dsDNA fragment libraries derived from each pool and subjecting them to multiplexed paired-end sequencing analysis on Illumina HiSeq 2000 platform (Supplementary Fig. 3). The use of multiple barcodes allowed us to analyze all aptamer pools in a single flow cell lane. We obtained a total of 1,180,685 raw sequences from all pools. During the initial bioinformatics analysis we observed a major decrease in sequence diversity of pools over the course of the selections, and an increase in copy numbers within the top, most frequent unique sequences indicating enrichment of target-specific binders. To identify β_2AR specific aptamers, we tracked the enrichment of individual sequences across successive selection rounds. This was performed by calculating the fold-enrichment for every sequence, which we defined as the ratio of percent frequency of a given sequence in the later round to that of the earlier round. We ranked RNA aptamer sequences by comparing fold-enrichment across multiple selection rounds and selected the top 20 sequences primarily based on their high enrichment ratios (Supplementary Fig. 4a; see online **Methods** for details). A scatter plot of fold-enrichments from R4 to R9 for the top 20-aptamer sequences in the selections against unliganded-β_2AR and β_2AR bound to BI167107 is shown in Figure 1b. Aptamer sequences skewed towards a particular axis are enriched and potentially selective towards that conformational state of the receptor.

RNA aptamers display conformation-specific binding

The 20 putative β_2AR binding aptamers were characterized for their binding to, and specificity, for unliganded β_2AR and β_2AR bound to BI167107 with ^{32}P-labeled and biotinylated aptamers, using nitrocellulose filter binding and pull-down assays, respectively (Supplementary Fig. 4). Several aptamers displayed varying levels of binding and specificity for the two selection β_2AR-targets (~75% of which bound to the receptor while 35% were conformation specific). These results are consistent with the data obtained from the deep sequencing analysis, which demonstrated multiple aptamer sequences displaying high fold-enrichment for the particular conformational state of the β_2AR that they are selected for (Fig. 1b and Supplementary Fig. 4). In the course of screening the initial 20 putative β_2AR binding aptamers, we obtained seven top aptamer candidates, which displayed robust β_2AR binding and/or conformational selectivity. These seven aptamers were further grouped into three categories as follows (Fig. 1b,c and Supplementary Fig. 4): (*i*) four aptamers (A1, A2, A12, and A13) showed conformational selectivity for the BI167107-bound or active form of β_2AR, (*ii*) two aptamers (A15 and A16) demonstrated binding specificity for the inactive form of β_2AR, and (*iii*) one aptamer, A11 did not show a clear selectivity, but bound to both unoccupied and BI167107-bound forms of the β_2AR with high affinity. In contrast to these aptamers, the control aptamer did not display significant binding to either conformational form of the receptor. *In silico* predicted secondary structures of these seven aptamers are shown in Supplementary Figure 5. Based on these screening results, the four candidate aptamers (A1, A2, A13 and A16) that showed strong conformational selectivity were selected for further characterization (boxed in Fig. 1c).

To further characterize these four aptamers, we measured the affinity and kinetics of their binding to active (BI167107-bound) and inactive (ICI-118,551-bound) forms of the β_2AR using a biophysical approach based on biolayer interferometry (BLI; ForteBio). BLI allows for quantification of the individual kinetic rate constants (k_{on} and k_{off}) that contribute to the equilibrium dissociation constants (K_d). We found that three aptamers (A1, A2 and A13) bound to β_2AR:BI167107 tightly with nanomolar affinities (K_d [A1] = 42.0 ± 2.3 nM, K_d [A2] = 258.5 ± 0.5 nM, and K_d [A13] = 30.4 ± 2.4 nM, respectively), with fast association rates and slow dissociation rates (Fig. 2 and see Supplementary Table 1 for kinetic parameters). In contrast, no detectable binding affinity to the β_2AR:ICI-118,551 was observed with these aptamers, indicating their specificity for an active conformation of the receptor. As expected, aptamer A16 bound to the β_2AR:ICI-118,551 with a nanomolar affinity (K_d [A16] = 93.1 ± 4.1 nM) but without any measurable affinity for the β_2AR:BI167107, demonstrating specificity towards an inactive conformation form of the β_2AR.

To investigate the influence of the four aptamers on the affinity of an agonist (isoproterenol) for binding to the β_2AR, we performed competition radioligand binding experiments with the radio-iodinated β-adrenergic antagonist cyanoiodopindolol ([^{125}I]-CYP) utilizing β_2AR reconstituted into high-density lipoprotein (HDL) particles[37]. As shown in Figure 3a, A13 promoted the greatest increase in the affinity of isoproterenol (ISO) for the β_2AR, 33.9-fold ([K_i] for [ISO + CNT-Apt] = 112 nM and for [ISO + A13] = 3.3 nM), followed by aptamer A1, which enhanced the affinity of isoproterenol for the β_2AR by 6-fold (K_i = 19.7 nM). In

contrast, the presence of aptamers A2 and A16 did not affect the affinity of the β_2AR for the agonist isoproterenol. Interestingly, although aptamer A2 had no effect on isoproterenol binding to the β_2AR, it did appear to recognize a receptor conformation stabilized by the agonist BI167107, suggesting it has the ability to distinguish between active conformations induced by two-full agonists, isoproterenol and BI167107. Similarly, aptamer A16 has no effect on agonist binding and appears to recognize only an inactive conformation of the β_2AR.

Next we explored the ability of these aptamers to modulate transitions between active and inactive conformations as well as whether they have the ability to stabilize unique ligand-specific conformations. To do this, we measured the ability of each aptamer to bind β_2AR occupied with a panel of pharmacologically and structurally distinct β_2AR ligands via a receptor pull-down assay using biotinylated-aptamers (chemical structures of the different β-adrenoceptor ligands used in this study are shown in Supplementary Fig. 6). We used three full agonists (BI167107, isoproterenol, and fenoterol), two partial agonists (salbutamol and clenbuterol), and four antagonists and inverse agonists (propranolol, carazolol, carvedilol, and ICI-118,551). Among these, carvedilol and BI167107 are modestly biased agonists towards β-arrestin-dependent signaling pathways[38,39]. Relative to the control aptamer, aptamers A1 and A13 robustly bound to agonist-occupied β_2AR, but this binding was significantly reduced in the presence of antagonists (Fig. 3b–e). Additionally, the binding specificity of these aptamers correlated directly with rank-order of agonist efficacy (Fig. 3b,d). Interestingly, we observed one aptamer, A2, whose effect on receptor binding did not correlate with ligand efficacy. With aptamer A2, we observed the largest receptor pull-down with BI167107-occupied β_2AR, and a slightly general selectivity trend towards agonist-occupied β_2AR conformations (Fig. 3c). Surprisingly aptamer A2 also displayed a unique selectivity towards a β_2AR conformation stabilized by carvedilol, among the antagonists. Aptamer A2's specificity for BI167107- and carvedilol-occupied β_2AR suggests that it stabilizes a unique active conformation of the β_2AR that is distinct from that stabilized by aptamers A1 and A13. In contrast to the other aptamers, A16 showed an opposite trend whereby it selectively stabilized antagonist-bound β_2AR complexes (Fig. 3e).

To obtain further insight into the ability of aptamers to stabilize active β_2AR conformations, we performed fluorescent spectroscopic studies on a β_2AR labeled with a bimane probe at the cytoplasmic end of TM6 at C265. The bimane probe enables direct monitoring of agonist-induced receptor conformational changes via TM6 movement from a hydrophobic environment to a more polar, solvent-exposed position as a decrease in fluorescence intensity (Supplementary Fig. 7). Both binding of agonist and G-protein (or its mimetic nanobody)[12,16] have previously been shown to alter the environment around the label, resulting in a decrease in fluorescence intensity and a rightward shift (red-shift) in emission λmax. Both the catecholamine agonist isoproterenol and high affinity agonist BI167107 induced conformational changes in the receptor thus changing the environment around the bimane label, as evidenced by the decrease in fluorescence intensity and a rightward shift in λmax (Fig. 4a–d). However, such changes were not observed in β_2AR occupied by an inverse agonist ICI-118,551. Interestingly, the effects of A1, A2 and A13 were enhanced (*i.e.*, a further decrease in fluorescence intensity and a rightward shift in emission λmax) when combined with full agonists, signifying further stabilization of active conformations

(Fig. 4a–c). No significant change in bimane fluorescence was observed with aptamer A16, consistent with its ability to recognize an inactive conformation of the receptor (Fig. 4d).

Functional effect of β_2AR aptamers

Stimulation of the β_2AR system promotes activation of the membrane-associated effector enzyme adenylyl cyclase (AC) via the stimulatory G protein subunit, $G\alpha_s$[40,41]. AC catalyzes the conversion of ATP to cyclic AMP (cAMP), one of the main second messengers of the GPCR signal transduction system. To determine the functional effects of the aptamers' binding to the β_2AR, we measured the ability of aptamers to modulate isoproterenol-stimulated $G\alpha_s$ and adenylyl cyclase activity by measuring the accumulation of cAMP (Fig. 5). Aptamers A13, A2, and A1 significantly inhibited isoproterenol-stimulated adenylyl cyclase activity by 46.1%, 34.7% and 28.3%, respectively ($p < 0.01$, $p < 0.01$, and $p < 0.05$, respectively *vs.* ISO-stimulated β_2AR; one way ANOVA). Aptamer A16 on the other hand was weaker and did not significantly alter the β_2AR-mediated adenylyl cyclase activity. The specificity of these inhibitory effects was further confirmed by the observation that the control aptamer had no effect on β_2AR-mediated adenylyl cyclase activity.

Molecular architecture of β_2AR-aptamer complexes

In addition to distinct properties, these functionally active aptamers appear to possess unique structural features. Specifically we characterized four aptamers that do not overlap with regard to sequence homology (Supplementary Fig. 4a) or predicted secondary structural motifs (Supplementary Fig. 5). In order to assess whether the aptamers bind at extracellular or intracellular regions of the β_2AR, we conducted a competition pull-down binding assay utilizing β_2AR-specific single domain nanobodies (Nbs) as competitive allosteric modulators. Both Nb80 (a G-protein mimetic nanobody) and Nb60 bind at the intracellular region around the G-protein binding cavity of the β_2AR, recognizing active and inactive conformations of the receptor, respectively[12,42]. The nanobodies were used in excess as competitors and the magnitude of competition (or cooperativity) was evaluated with corresponding aptamers based on the level of captured β_2AR (pre-bound with either BI167107 or ICI-118,551). As illustrated in Supplementary Figure 8a, Nb80 strongly inhibits the interaction of A1 and A2 with the activated β_2AR, consistent with substantial overlap between the binding sites of Nb80 and those of aptamers A1 and A2. In contrast, Nb80 increases the interaction of activated β_2AR with aptamer A13, suggesting a positively cooperative effect and minimal overlap between the binding sites of Nb80 and aptamer A13. Likewise, Nb60 enhanced the binding of inactive β_2AR to aptamer A16, indicating the possibility of cooperativity and lack of competition between the two, consistent with the presumption that aptamer A16 may be binding at the extracellular region of β_2AR (Supplementary Fig. 8b).

To gain further insight into the binding epitopes and structural basis of the interactions between the aptamers and different β_2AR conformations, we next used negative stain transmission electron microscopy (EM) and single-particle reconstruction analysis[43,44]. After successfully visualizing the aptamers in complex with the receptor via EM, we further improved the visualization and post-imaging analysis alignment, through increasing the size of the complex to help us identify whether the aptamers were interacting with the

extracellular or intracellular surface of the receptor. Improved EM imaging was achieved by affinity purifying samples of β_2AR-ligand-aptamer complexes labeled with anti-Flag antigen-binding fragment (Fab), derived from a monoclonal antibody that recognizes the FLAG epitope located at the extracellular N-terminus of the receptor[39] (Supplementary Fig. 9a,b and online **Methods**). From the EM two-dimensional class averages, we identified a central oval density, as the receptor embedded in the MNG detergent micelles (for receptor alone see Supplementary Fig. 9c). Furthermore, in the EM particle averages, the Fab is shown to bind exclusively to the extracellular N terminus of the β_2AR and serves as a landmark to help locate the aptamer binding domains on the receptor (see Supplementary Fig. 9d for Fab-β_2AR complex and Supplementary Fig. 9e for a representative aptamer-β_2AR complex). By comparing the Fab-β_2AR complex class averages with those of complexes bound to aptamers, we were able to identify densities corresponding to aptamers in complex with receptor (Supplementary Fig. 9f and Fig. 6). As illustrated in the 2D-class averages of the β_2AR complexes bound to aptamers A1, A2 and A13, the binding locations (densities) corresponding to each of the aptamers appear localized on the side opposite to (or distant) from the Fab, suggesting that aptamers A1, A2 and A13 bind at the intracellular region of the β_2AR (Fig. 6a–c). On the other hand, by virtue of its binding on the same side as the Fab, A16 appears to interact with the extracellular region of the receptor (Fig. 6d).

DISCUSSION

In recent years within the field of GPCR signaling a large body of work has emerged exploring the underlying structural determinants of ligand-receptor interactions associated with pathway-specific functionally relevant receptor conformations. Characterizing such ligand-selective signaling conformations could serve as the basis for the design of GPCR ligands with better efficacy, improved safety profile, and an enhanced therapeutic window. Elucidating the structural and mechanistic features of these conformations using currently available tools has been challenging, in part due to the inherent flexibility of GPCRs and the fact that X-ray crystallography tends to capture thermodynamically stable inactive conformations[9,15,17,18,45]. These challenges have underscored the need for the development of conformationally selective allosteric agents that can stabilize distinct active and inactive receptor conformations. Although antibody-mediated stabilization of GPCRs or other proteins is a formidable advance[12,13,46–48], its widespread utility remains limited by problems associated with immunogenicity, economic feasibility, and the time-consuming nature of immunization and library construction. Due to vast library diversity attainable for selections, the nature of chemical compositions of nucleotides, and the unique 3D–conformations they can attain, RNA aptamers have great potential as valuable conformation-sensors and pharmacologic agents for GPCRs[19–32].

Herein, we describe the development of state-selective RNA aptamers that allosterically stabilize different conformations of the β_2AR. Our results reveal that the aptamers have distinct preferences for binding specific receptor conformations with nanomolar range affinities (Fig. 2 and Supplementary Table 1). We utilized a targeted selection method that allowed for enrichment of RNA aptamers that selectively bind distinct active and inactive receptor conformations. In addition, our approach here also employed NGS and comparative bioinformatics analyses to monitor the complexities of selected pools and the dynamics of

enrichments of unique sequences (via evaluation of fold-enrichment) to derive state-selective aptamers (see online **Methods**). Our analysis, primarily based on fold-enrichment of individual RNA clones, is capable of discerning which aptamers were strongly enriched by each specific β_2AR target. Notably, these aptamer modulators would not have been identified by traditional clonal selection strategies that pick the most abundant clones since non-specifically binding aptamers could dominate the selected population. Together, the aptamers that we isolated demonstrate the effectiveness of the selection strategies and NGS analysis applied here in identifying aptamer modulators for the β_2AR, which may have been obscured using traditional clonal selection strategies.

Selectivity of the aptamers for specific β_2AR conformations also correlated with receptor ligand efficacy as demonstrated using biochemical, pharmacological and biophysical approaches. Of the aptamers, A1, A2, and A13 showed strong conformational selectivity for the high-affinity agonist (BI167107)-bound active β_2AR conformation, while aptamer A16 displayed conformational selectivity for the inverse-agonist (ICI-118,551) inactive β_2AR conformation. Interestingly, while both aptamers A1 and A13 allosterically enhanced agonist (isoproterenol) binding affinity and bound the receptor in an agonist dependent manner, aptamer A2 appeared to have a unique ligand specificity with preferential binding to BI167107, and to a lesser extent, to carvedilol-bound β_2AR states. Both BI167107 and carvedilol have been shown to act as modest β-arrestin-biased ligands at the β_2AR[38,39]. This result may therefore, suggest there is possible overlap between the conformational states stabilized by BI167107 and carvedilol, and that aptamer A2 may recognize a unique ligand-induced, potentially β-arrestin-biased conformation of the β_2AR. The influence of aptamers on agonist-induced receptor conformational changes was also assessed in a fluorescence spectroscopic study using bimane probe on TM6[12,16]. Indeed, three of the aptamers (A1, A2 and A13) enhanced agonist induced conformational rearrangement of TM6, consistent with their ability to stabilize active receptor conformations via a positive cooperative interaction between β_2AR and the aptamers. Conversely, aptamer A16 had little to no influence on the movement of TM6, in particular for the BI167107-bound state of β2AR, consistent with its ability to stabilize an inactive conformation of the β_2AR.

Stimulation of the β_2AR activates heterotrimeric G-proteins and increases the rate of guanosine diphosphate/guanosine triphosphate (GDP/GTP) exchange on the Gα subunit to mediate the activation of adenylyl cyclase (AC) with subsequent accumulation of cAMP[40,41]. Interestingly, aptamers A1, A2, and A13 significantly inhibit agonist-induced cAMP accumulation. It has previously been shown that binding of intracellular-expressed antibodies to β_2AR inhibits receptor-mediated downstream signaling at the G-protein binding site[42]. We hypothesize that the potential mechanism of inhibition of β_2AR-mediated AC activity by aptamers (A1, A2 and A13) is likely secondary to their binding at the intracellular region of the receptor with resultant steric blockade of G protein binding. The lack of significant inhibition of AC activity by aptamer A16 may be attributed to its relatively weak binding affinity for the receptor. The recognition of functional activity of these aptamers is intriguing with regard to their potential use as pharmacological agents targeting GPCRs. Indeed, aptamers have been developed to bind many drug targets and constitute potential therapeutic agents as exemplified by the first aptamer-based drug for

macular degeneration (pegaptanib sodium) as well as others that have undergone clinical trials[19–23]. Although we only identified ligands that inhibit agonist activity, the diversity of RNA libraries suggests it may be possible to identify receptor aptamers with diverse functionalities ranging from agonists to positive and negative allosteric modulators.

GPCRs are versatile allosteric machines and their signaling activities can be affected by the binding of modulators at distinct sites. Indeed, several allosteric sites have been described recently, encompassing regions of the extracellular and intracellular surfaces for GPCRs, including the β_2AR[49,50]. Interestingly, none of the antibody-based allosteric modulators reported for the β_2AR bind at the extracellular region[12,42]. Our EM analysis[43,44] and competition studies using β_2AR specific nanobodies[12,42] revealed the architecture of the β_2AR-aptamer complexes and the location of the interaction epitopes of the aptamers on the surface of the receptor. Notably, using EM the BI167107-bound Fab-β_2AR-aptamer complexes (A1, A2 or A13) show densities for the aptamers located opposite to the reference anti-FLAG Fab, suggesting their binding at the intracellular region of the receptor. EM images obtained for ICI-118,551-bound Fab-β_2AR-A16 on the other hand suggest that it interacts with the extracellular region of the receptor. The EM data is consistent with the hypothesis that the aptamers potentially act through engagement via allosteric mechanisms involving key structural elements of the allosteric sites located at either the intracellular or extracellular regions of the receptor.

In summary, the present study illustrates that aptamers can act as allosteric modulators by distinguishing between receptor conformations stabilized by pharmacologically different ligands. Our results therefore establish the potential of RNA aptamers to serve as allosteric modulators for elucidating the structural and mechanistic aspects underlying GPCR activation and signaling. In addition, by virtue of the ability of aptamers to lock receptors in biologically relevant conformations of interest, aptamers may also play a role in small-molecule drug discovery efforts for identifying allosteric modulators against said conformations. Furthermore, given their favorable pharmacologic characteristics, relative tolerability for progression to the market[19–23], and broad library diversity, RNA aptamers could represent an attractive class of GPCR ligands. Finally, the general approach used here establishes a framework for developing aptamers aimed at a wide range of soluble and membrane proteins that undergo function-dependent conformational changes.

ONLINE METHODS

Reagents

Sf9 cell culture media and transfection kits to generate virus stocks were purchased from Expression Systems. BI-167107[36], synthesized as described previously[36], was a generous gift from Dr. Xin Chen (Changzhou University, Changzhou, Jiangsu, China). All other ligands were purchased from Sigma-Aldrich. Other reagents were of analytical grade obtained from various suppliers and used without further purification unless indicated otherwise.

Expression and purification of recombinant proteins

Human β_2AR containing an N-terminal FLAG epitope tag, C-terminal 6xHis-tag, and a N187E glycosylation mutation was expressed in Sf9 insect cells using the BestBac Baculovirus Expression System as described previously[4]. Briefly, cells were infected with β_2AR baculovirus at a density of 3×10^6 cells/mL and harvested 67 hours later. Next, cells were lysed using a lysis buffer [10 mM Tris, pH 7.4, benzamidine (10 mg/mL), leupeptin (10 mg/mL)] and subsequently solubilized in an *n*-Dodecyl-β-D-maltoside (DDM; Anatrace) containing solubilization buffer [1.0% DDM, 500 mM NaCl, 20 mM Tris, pH 7.4, benzamidine (10 mg/mL), leupeptin (10 mg/mL), PMSF (200 μmol)]. Functional β_2AR was obtained using a three-step affinity-chromatographic procedure involving a first M1 anti-FLAG-antibody affinity column, followed by alprenolol-ligand column and a second M1 anti-FLAG antibody-affinity column[4]. The alprenolol-ligand affinity purification step selectively isolates functional receptors from those non-functional ones that are incapable of binding radioligand ^{3}H-dihydroalprenolol. In the second anti-FLAG affinity chromatography, DDM was exchanged to MNG (Anatrace), for increased stability, by a gradual gradient of DDM:MNG buffer containing 0.001% (w/v) cholesterol hemisuccinate (CHS). FLAG-tagged β_2AR was incorporated into high-density lipoprotein (HDL) particles using membrane scaffold protein 1, a derivative of apolipoprotein A-I[51], as previously described. Briefly, FLAG-tagged β_2AR was incubated with a 50-fold molar-excess of MSP1, 8 mM POPC:POPG (3:2 molar ratio; 1-palmitoyl-2-oleoyl-sn-glycero-3-phosphocholine and 1-palmitoyl-2-oleoyl-sn-glycero-3-phospho-[1'-rac-glycerol]) lipids (Avanti Polar Lipids) for 1 hour at 4 °C. After removal of detergent using BioBeads SM-2 (Bio-Rad) overnight at 4 °C, receptor-containing HDL particles were purified by M1 anti-FLAG antibody-affinity column followed by size-exclusion chromatography. Receptors in HDL particles are generally stable and suitable for performing radioligand-binding experiments. Similarly as for the β_2AR, FLAG-tagged (N-terminus) and hexahistidine-tagged (C-terminus) human angiotensin-receptor subtype 1a (AT1aR) with T4-lysozyme insertion in the third-intracellular loop (between Y229 and E230) was expressed in baculovirus-infected Sf9 cells and solubilized in 1% (w/v) DDM. Receptor (in presence of telmisartan) was purified by Ni-NTA-resin, followed by M1 Anti-FLAG antibody-affinity chromatography. Expression and purification of His-tagged nanobodies was performed as described previously[42].

DNA templates, synthesis of 2′-F-pyrimidine RNA transcripts, and biotinylated RNA aptamers

The starting double-stranded DNA (dsDNA) library was composed of individual sequences of 107 nucleotides long, including flanking constant regions and a variable region containing 40 nucleotides as described by the following example: 5′-GGGGGAATTCTAATACGACTCACTATAGGGAGGACGATGCGG-N_{40}-CAGACGACTCGCTGAGGATCCGAGA-3′. The final sequence complexity of our dsDNA library was ~10^{15} unique sequences. A single-stranded DNA template library was converted to the dsDNA while introducing the T7 promoter (underlined sequence) by annealing with Klenow exo- (NEB), library 3′ template oligo, 5′-TCTCGGATCCTCAGCGAGTCGTCTG-N_{40}-CCGCATCGTCCTCCCTA-3′ and the 5′-primer oligonucleotide, 5′-GGGGGAATTCTAATACGACTCACTATAGGGAGGACGATGCGG-3′. The resulting

library was later PCR amplified using Taq DNA polymerase (Life Technologies), 5′-primer, and the 3′-primer, 5′- TCTCGGATCCTCAGCGAGTCGTC-3′. A combinatorial library of chemically modified 80-nucleotide RNA (~10^{15} unique sequences) was created by transcription of the randomized DNA oligonucleotide using Y639F mutant T7 RNA polymerase that allows incorporation of 2'-fluoro modified pyrimidines. Double-stranded DNAs representing RNA pools or individual aptamers were directly used for overnight *in vitro* transcription at 37 °C in transcription buffer containing a mutant T7 RNA polymerase Y639F, 2′-hydroxyl normal purine nucleotides (ATP and GTP each at 1 mM; Roche), and 2′-deoxy-2′-fluoro pyrimidine nucleotides (2′-Fluoro-modified CTP and UTP, each at 3 mM; Trilink). All transcription reactions involving libraries or individual RNAs were performed using 2′-fluoro-CTP and 2′-fluoro-UTP, to generate RNAs that were resistant to extracellular RNases[52]. RNA transcription reactions were treated with DNase I (Roche) to remove dsDNA template, phenol-chloroform extracted, and concentrated using centricon 10 in TE buffer [10 mM Tris, pH 7.4, 0.1 mM EDTA]. The concentrated RNAs were purified with polyacrylamide gel electrophoresis, 7 M urea, 0.5x Tris borate EDTA (TBE) gel. The RNA aptamers were then visualized by UV shadowing, excised from the gel, eluted in 5 mL of TE buffer at 37 °C for 3 hr. 5′-end biotinylated RNA aptamers were generated similarly, by performing *in vitro* 2′-F RNA transcriptions with 5′-Biotin-G-Monophosphate at 3 mM (GMP; TriLink)[52].

Aptamer cloning and sequencing

Individual dsDNA forms of the RNAs were prepared by annealing, amplifying using PCR, and sub-cloning them as described above. The template DNA oligonucleotide for each aptamer was purchased from Integrated DNA Technologies. The starting dsDNA sequences (107 base-pair-long) of aptamers were generated by annealing template oligonucleotide (specific for each aptamer), 5′-TCTCGGATCCTCAGCGAGTCGTCTG-N_{40}-CCGCATCGTCCTCCCTA-3′ and the 5′- primer oligonucleotide, 5′-GGGGGAATTCTAATACGACTCACTATAGGGAGGACGATGCGG-3′. Each annealed oligonucleotide was filled in with Klenow exo- and purified. The dsDNA products of desired aptamers or aptamer pools were cloned into pCR 2.1-TOPO vector cloning vector (Life Technologies), transformed into *E. coli* and sequenced (Eton Bioscience).

In vitro selection of aptamers

RNA aptamers were generated using a Systematic Evolution of Ligands by Exponential Enrichment (SELEX)[31] procedure against purified β_2AR that was either unliganded or BI167107-bound. The selection library consisted of 80 nucleotide-long RNA oligonucleotides with a central random region of 40 nucleotides, flanked by constant regions of a 15-base 5′-primer sequence and a 25-base 3′-primer sequence. The RNA library in selection buffer (20 mM HEPES, pH 7.4, 50 mM NaCl, 2 mM $MgCl_2$, 2 mM $CaCl_2$) was heat denatured at 65 °C, slowly cooled to room temperature (RT), and supplemented with MNG and CHS at final concentrations of 0.01% (w/v) and 0.001% (w/v), respectively. The RNA library solution was mixed with the nitrocellulose matrix, FLAG-peptide (0.5 μM), with or without BI167107, for selection against β_2AR or β_2AR-BI167107, respectively. The mixtures were incubated for 30 min at 25 °C, prior to every round of selection with unliganded or β_2AR-BI167107, to remove nonspecific target-binding species. In the

negative-selection step during the fifth round, the RNA library was incubated with a non-target receptor (50 nM of AT1aR bound to 10 μM telmisartan). The pre-cleared RNA libraries (2.25 nmole) were recovered and then incubated with respective target protein, either unliganded or BI167107-bound β_2AR (1.125 μM; RNA/receptor ratio 5/1) for 30 min at 25 °C in 400 μL selection buffer on a rotating wheel. Starting from round 2, yeast tRNA (20 ng/μL) was used in the selection mixture to eliminate nonspecific binding. After incubation, the selection mixtures were passed through nitrocellulose filters to capture β_2AR-RNA complexes and remove supernatant containing unbound aptamers. Bound RNA molecules were then incubated in phenol:chloroform:isoamyl alcohol for 30 minutes at RT, chloroform extracted, ethanol precipitated, and resuspended in TE buffer (10 mM Tris pH 7.4, and 0.1mM EDTA) to extract the RNAs from the membrane. One-quarter of the extracted RNA was reverse transcribed (RT) with 3′ primer, dNTPs, and AMV Reverse Transcriptase (Roche). The RT reaction was PCR amplified with the 5′ and 3′ primers described above using platinum *Taq* polymerase and standard PCR conditions. The PCR reactions were desalted and excess reagents were removed using Centricon 30 (Millipore) and washed with TE buffer. The dsDNA products were then used to generate RNA pools for the next round using *in vitro* transcription as described above. Nine rounds of selection were performed, and selection pressure was increased throughout the process as follows: i) Ionic strength (concentration of NaCl) was 50 mM for the rounds1 to 3, 75 mM for the rounds 4 to 6, and 100 mM for the rounds 7 to 9; ii) The amount (nmoles) of RNA library input was decreased to 1, 0.5 and 0.25 in rounds 2, 5, and 8, respectively and the aptamer:β_2AR ratio was 5:1 for the rounds 1 to 4, 7:1 for the rounds 5 to 7, 10:1 for the rounds 8 and 9. Filter-binding assay was used to evaluate the binding affinity of the individual selected pools (see below).

High-throughput next-generation sequencing (NGS) of RNA aptamer pools

To determine the sequences enriched through *in vitro* selection, we performed high-throughput next-generation sequencing (NGS) using HiSeq 2000 (Illumina). Each RNA pool was reverse transcribed using AMV Reverse Transcriptase (Roche), by substituting the 3′-primer with the appropriate NGS 3′-primer that has 6-bases barcode and NKKNKK region (Supplementary Fig. 3). The cDNA for each selection round was amplified by PCR using Phusion Hot Start II High-Fidelity DNA Polymerase (Thermo Scientific) with 5’ and 3’ primers containing barcode (6-base Illumina-compatible unique DNA barcodes for each pool), NKKNKK region, and 12-base complement sequences of the original constant regions of dsDNA PCR selection primers. The NKKNKK sequence facilitates cluster identification and ensures generation of high quality reads during Illumina sequencing (a common remedy for Illumina amplicon low diversity issue) while the 6-base pair barcode sequence, unique for each pools, helps identify each pool during multiplex sequencing. The resulting barcoded PCR products were purified with QIAEX II Gel Extraction Kit and QIAquick PCR purification Kit protocols. The DNA fragment libraries (94-bp; Illumina-compatible dsDNA fragments) were further purified and concentrated using phenol-chloroform and ethanol-precipitation. The products were then ligated with the adapters (which included end-repair, A-tailing and paired-end adapter ligation), amplified by cluster generation and processed for NGS according the protocols provided by Illumina, Inc. Final library sizes were determined using the Agilent Bioanalyzer and quantified using the Qubit

(Life Technologies). Indexed DNA samples were pooled together with equal molar-ratios and used for multiplex sequencing. High-throughput sequencing from both ends of the library inserts (*i.e.*, paired end sequencing) was performed by the sequencing core facility at Duke Center for Genomic and Computational Biology, Duke University.

Bioinformatics and *in silico* methods for sequence analysis

Raw paired-end reads from each pool were processed to: 1) remove low quality paired-end reads and adapters using CutAdapt (http://journal.embnet.org/index.php/embnetjournal/article/view/200) 2) the first 6 random sequence that was designed to remedy amplicon low diversity issue was also trimmed similarly 3) demultiplex and identify each pool of multiplex pooled sample using FASTX-Toolkit (http://hannonlab.cshl.edu/fastx_toolkit/links.html). A custom Perl script was developed in-house for downstream data processing and analysis that 1) extracts the sequence of interests (random regions of interests) by removing the constant sequences that contain barcodes and PCR primers at the 5' and 3' regions, 2) clusters the resulting sequence (individual clonal sequences) based on sequence identity to generate a unique set of the sequences, 3) calculates the frequency and percentage of frequency of each unique sequence, and 4) transcribes the nucleotide sequences of the individual sequences into RNA sequences for downstream analysis. We used the frequency and percentage of frequency of each unique sequence in individual selection pools to compute enrichment-ratios between two rounds. Fold-enrichment of unique sequences was calculated by dividing percent frequency of the later round by that of the earlier round. We used fold-enrichment to account for the aptamers that might have had a low copy number, but still had relatively high numbers in the next round of selection. Secondary to this reason, we think the use of enrichment-ratios of individual sequences rather than copy number provides higher resolution characterization of pools and dynamics of enrichment of unique sequences, and thus, has significant advantage in the end in ensuring efficient and successful isolation of target specific binders. RNA sequences were ranked according to their fold-enrichment across successive rounds and their enrichment dynamics were evaluated. To help us narrow candidate list that we could synthesize and test, next, we performed further bioinformatics analyses for the top ranking aptamers using combinations of tools including Microsoft Access, Microsoft Excel, GraphPad Prism, MacVector (MacVector, Inc.), Clustal Omega (http://www.ebi.ac.uk/Tools/msa/clustalo/), and RNA folding algorithm *Mfold* (http://unafold.rna.albany.edu/?q=mfold). The analyses include primary sequence alignments and comparisons between them to pick the representative of each cluster; analysis of the relative structural stability of individual sequences from minimal energies computed from the secondary structure predictions; scatter plot analysis of fold-enrichments between the two selection types; and rank-order copy numbers (*e.g.*, at R6 and R9 selected pools). Based on these analyses we selected 20 top candidate aptamers to be cloned and synthesized as a 5′-end biotin moiety or radio (^{32}P)-labeled RNA aptamer versions, to subsequently evaluate their binding with the selection targets.

Radiolabeling of RNA aptamers

RNA aptamers were radioactively labeled by ^{32}P at the 5′-end, initially by removing the 5′-terminal phosphate group with bacterial alkaline phosphatase (Life Technologies) at 65 °C for 1 hr and then purifying them by phenol/chloroform extraction followed by ethanol

precipitation. 3 pmol of each dephosphorylated aptamer was incubated with ^{32}P-labeled γ-ATP and T4-polynucleotide kinase (NEB) at 37 °C for 45-minute. Radiolabeled aptamers were finally purified using G25-spin column (GE Healthcare) following the manufacturer's instructions. Incorporated radioactivity was quantified using a scintillation isotope counter.

Filter binding assay

The binding affinities of the different RNA pools or individual aptamers were determined by nitrocellulose-membrane filtration-based saturation binding assay. Constant amounts of 5′-[^{32}P]-radiolabelled RNA aptamers (at 2000 CPM/μL final) were incubated with increasing concentrations of the β_2AR or β_2AR:BI (12 two-fold serial dilutions starting from 2 μM) in a buffer containing 20 mM HEPES, pH 7, 50 mM NaCl, 2 mM $MgCl_2$, 2 mM $CaCl_2$, 0.01% MNG and 0.001% CHS for 30 minutes at RT. The final reaction volume was 20 μL. The β_2AR-RNA aptamer mixtures were then passed through a stack of membranes on a vacuum-manifold consisting of a Protran-nitrocellulose that captures RNA-protein complexes and GeneScreen Plus® nylon membrane that captures unbound RNA molecules. After washing twice with 100 μL binding buffer the membranes were air dried for 5 minutes, exposed to Phosphoimager screens (1 hr), and scanned using a Molecular Typhoon Phosphoimager (GE Healthcare). Finally, the fraction of RNA-bound was calculated, adjusted for background and graphed using GraphPad Prism. The equilibrium dissociation constant (K_d) for the RNA aptamers were obtained by fitting the fraction of nitrocellulose-bound RNA to the following equation: $Y = (B\text{max}*X) / (X + K_d)$, where Bmax is the maximum value of Y (when X = ∞); and K_d, the dissociation constant, is the value of X when Y = Bmax /2.

Pull-down experiments

In order to measure the binding activity of aptamers to the β_2AR, we pulled down receptors using NeutrAvidin-beads (Pierce) by immobilizing biotinylated aptamers. Beads were first incubated in blocking buffer [20 mM HEPES, pH 7.4, 100 mM NaCl, 2 mM $MgCl_2$, 2 mM $CaCl_2$, 0.1% BSA] at 4°C to block non-specific binding sites. Biotinylated RNA aptamers in HNKMC buffer [20 mM HEPES, pH 7, 25 mM NaCl, 5 mM KCl, 5 mM $MgCl_2$, 2 mM $CaCl_2$] were heat denatured at 65 °C for 5 min and cooled down to RT for proper re-folding into their native conformations. Biotinylated RNA aptamers, each at 2.5 μM concentration, were then immobilized onto 25 μL NeutrAvidin beads in HNKMC buffer with 0.01% MNG and 0.001% CHS for 20 min at RT with rotation. The bead-aptamer mixtures were subsequently incubated with β2AR (final concentration at 250 nM) that has a carrier solvent or indicated ligand (final concentration at 25 μM) for 1 hr at RT in a 125-μL total reaction volume. For nanobody competition studies, pull-down experiments were performed as described here with minor adjustments. Intracellularly acting β2AR-specific nanobodies (Nb80 and Nb60, a positive and negative allosteric modulators, respectively) were used to assess cooperativity and competition with the aptamers. 10 ìM of nanobody (Nb80 or Nb60) or buffer alone was mixed with receptor (pre-reacted with carrier solvent, ICI-118,551 or BI167107) and added to bead-aptamer mixtures. In both cases after incubation, the receptor complexes (with or without aptamer and/or nanobody) were centrifuged and unbound mixtures were washed three times. Bound complexes were eluted with 37.5 μL buffer containing 20 mM HEPES, pH 7, 100 mM NaCl, 250 mM DTT, 500 μM Biotin and 50 mM EDTA for 20 min at RT. 12.5 μL of 4x SDS sample buffer was added to each eluted sample

prior to performing a Western blotting using anti-β2AR antibody (sc-569; Santa Cruz), and ethidium bromide (EtBr) staining for RNAs on a 10% TBE gel (Life Technologies).

Binding affinity measurements by biolayer interferometry (BLI)

The kinetics of interactions of aptamers (A1, A2, A13, or A16) with the BI167107 or ICI-118,551-bound β_2AR were measured by BLI on a ForteBio's Octet RED96 System. Prior to immobilization the biotinylated aptamers were incubated at 65°C for 5 min and then cooled to RT. Biotinylated aptamers were then immobilized onto Streptavidin (SA) biosensor tips (FortéBio) in a buffer composed of 20 mM HEPES, pH 7, 25 mM NaCl, 5 mM KCl, 5 mM $MgCl_2$, and 2 mM $CaCl_2$ by dipping the SA sensors into wells containing biotinylated aptamers for 600 seconds. The loading levels of aptamers were kept between 1 and 1.2 nm in screening assays and between 0.2 and 0.35 nm for titrations. The aptamer-loaded sensors were washed with buffer for 60 seconds. After obtaining baseline in the buffer that contained 0.01% MNG and 0.001% CHS, the association of BI167107 or ICI-118,551-bound β_2AR (at a 1:20 receptor to ligand ratio) at varying concentrations was monitored for 300 seconds, followed by dissociation into the buffer for 300 seconds. Aptamer-free blank SA sensors were used in parallel to record signals due to non-specific interactions, which were subtracted out to obtain specific binding data. Signal from the interaction between receptor-free buffer with 0.01 % MNG and sensors was used to double reference to remove drifts in specific binding data. The association and dissociation rate constants (k_{on} and k_{off}) and the dissociation constant (K_d) values were obtained by fitting the aptamer specific binding data globally to a 1:1 Langmuir binding model using FortéBio's Data Analysis software 7.1.0.36 (ForteBio) and/ or BiaEval 4.1 programs.

Competitive radioligand binding experiments

Competition radioligand binding assays were performed with purified β2AR reconstituted into HDL particles (nanodiscs) and radioiodinated cyanopindolol ([^{125}I]-CYP (2200 Ci/mmol; PerkinElmer). Binding experiments (150 μL) contained 60 pM [^{125}I]-CYP, a serial dilution of competitor (isoproterenol), aptamers (2.5 μM), and β_2AR in HDL (~ 0.6 ng) diluted in assay buffer (20 mM HEPES pH 7, 20 mM NaCl, 5 mM KCl, 10 mM $MgCl_2$, 2 mM $CaCl_2$, 0.05% BSA, 1mM L-ascorbic acid). Aptamers were first heat denatured at 65 °C for 5 min and then cooled at RT. After a 90 min incubation at RT, binding assays were terminated by vacuum filtration through GF/B glass-fiber filters treated with 0.3% polyethylenimine and washed three time with cold buffer using a harvester (Brandel). Total binding was measured in the absence of competitor and nonspecific binding was determined in the presence of 10 μM propranolol. Radioligand binding was measured in a Packard Cobra Quantum gamma counter (Packard). All results are from at least three independent experiments. Fifty percent inhibitory concentrations (IC_{50}) were determined by fitting the data from the competition studies to nonlinear regression analysis (one-site competition model) using Prism (GraphPad Software).

Bimane fluorescence spectroscopy

β_2AR (minimal cysteine version with mutations: C77V, C327S, C378A, and C406A) purified as described above was labeled with monobromobimane (mBBr) (Life Technologies) at Cys265 on TM6. Labeling was performed at a 1:2.5 receptor-mBBr molar

ratio in buffer (20 mM HEPES pH 7.4, 100 mM NaCl, 2 mM $MgCl_2$, 2mM $CaCl_2$, 0.01% MNG and 0.001% CHS) overnight on ice in the dark. Labeled receptor was purified by gel filtration. RNA aptamers were prepared in HNKMC buffer [20 mM HEPES, pH 7, 25 mM NaCl, 5 mM KCl, 5 mM $MgCl_2$, 2 mM $CaCl_2$] and heat denatured at 65 °C for 5 min and then cooled down at RT. To determine the effect of aptamers, spectra were taken after 30 min incubation of bimane-labeled receptor (2 μM) at RT with or without isoproterenol (ISO; 200 μM), BI167107 (BI; 200 μM), ICI 118551 (ICI; 200 μM) or aptamers (4 μM), or a combination of a ligand and an aptamer. Fluorescence spectra were read in a SpectraMax M5 plate reader (Molecular Devices) using an excitation wavelength set at 370 nm and emission range from 430 to 600 nm in 1-nm increments. Spectra were corrected for background intensity from buffer, ligands and aptamers. Fluorescence emission curves fit to normal distribution were drawn using Prism.

Adenylyl cyclase (AC) activity assay

The effect of aptamers on β2AR-dependent stimulation of AC activity was assessed by 3', 5'-cyclic AMP (cAMP) accumulation on HEK-293 membrane homogenates stably expressing β_2AR[53] (a clone developed in the laboratory that has an expression level of ~ 2 pmoles/mg), by measuring the conversion of [α-^{32}P]-ATP to [α-^{32}P]-cAMP as previously described[54]. Typical assay setup contained a final total volume of 100-μL, performed in 3-steps. First, a premix sample (with or without ligand) of 60 μL consisting of final concentrations of 50 mM Tris-HCl, pH 7.5, 5 mM $MgCl_2$, 1 mM ATP, 1 μM GTP, 1 mM cAMP, 2 μCi [α-^{32}P]-ATP, ATP-regenerating system [20 mM creatine phosphate and 13 units/100 μL of creatine-phosphokinase], and phosphodiesterase inhibitors [250 μM of Ro 20–1724 and 100 μM of 3-isobutyl-1-methylxanthine] with or without 100 nM isoproterenol were mixed. Second, HEK-293 membrane homogenates (150 μg) were incubated with individual aptamers (4 μM; heat denatured and refolded as described above) or assay buffer alone in a total volume of 40 μL for 20 min on ice. Then, to measure AC activity in response to isoproterenol (100 nM) or isoproterenol (100 nM) in combination with aptamers (4 μM), the premix samples (60 μL) and membrane mixtures (40 μL) were incubated at 37 °C for 10 min. Reactions were terminated with 0.8 mL cold trichloroacetic acid (6.25% wt/vol); and 100 μL of [^{3}H]-cAMP (~25,000 cpm) was added as a recovery marker. Samples were pelleted by centrifugation at 1,500 × g for 20 min at 4°C. The [α-^{32}P]-cAMP formed was then isolated from the remaining ATP by applying the 1 mL reaction mixture to a sequential chromatography using a Dowex gel column followed by filtration on an aluminum oxide column and elution with 4 mL of 0.1 M imidazole, pH 7.5. The samples were counted for both ^{3}H and ^{32}P, and the counts were converted to AC activity as picomole of cAMP/mg of protein/min as described previously[54].

Specimen preparation and EM imaging of negative-stained samples

To prepare for EM visualization of the β_2AR-aptamer complexes, affinity-purification using biotin/NeutrAvidin system was employed, as described above, for pull-down assays. An anti-FLAG Fab was developed to specifically label the FLAG-tagged β_2AR at its extracellular N-terminus. This Fab was derived from a monoclonal mouse anti-FLAG M1 IgG that recognizes the FLAG-epitope was produced using hybridoma technology for antibody production[43]. The anti-FLAG Fab was isolated by digestion of the monoclonal

mouse anti-FLAG M1 IgG on an immobilized-papain protease resin and followed by purification on a Protein-A column (Pierce)[43]. The β_2AR and aptamer complexes (assembled as 10 μM and 20 μM in 125 μL volume, respectively) were formed in a buffer composed of 20 mM HEPES, pH 7, 25 mM NaCl, 5 mM KCl, 5 mM $MgCl_2$, 2mM $CaCl_2$, 0.01% MNG, 0.001% CHS and 10 μL ligand. β_2AR-aptamer complexes were eluted in a buffer that has 4 mM biotin and then prepared for EM using conventional negative-staining protocols as described previously[44]. Specimens were imaged at RT with a FEI Tecnai G^2 Twin electron microscope operated at 120 kV using low-dose procedures. Images were recorded at a magnification of ×65,200 and a defocus value of ~1.5 μm on an Eagle 2K CCD camera.

Two-dimensional classification

Two-dimensional EM reference-free alignment and classification of particle projections were performed using ISAC[44]. Particles were both automatically and manually excised using Boxer (part of the EMAN 2.1 software suite)[44]. Over 10k 0° particle projections of either β_2AR alone, β_2AR-aptamer (A1, A2, A13 or A16), Fab-β_2AR, or Fab-β_2AR-aptamer (A1, A2, A13 or A16), were subjected to ISAC, producing at least 50 classes. Given the challenge of observing aptamers via EM due to their small size, our goal was to identify the particle averages, which allowed visualization of the β_2AR-aptamer interaction. Approximately 5–10% of the particle averages demonstrated β_2AR-aptamer interaction. To determine β_2AR-aptamer conformations, each class average was designated as ‘receptor alone’, ‘receptor-aptamer’ or ‘unassigned’ and the number of projections resulting in ‘receptor-aptamer’ complex formation were utilized (relative to Fab-tag) to help identify extracellular versus intracellular interactions.

Statistical analysis

Statistical analysis and curve fitting were done using Prism 6 (GraphPad Software). For statistical comparison, one-way analysis of variance (ANOVA) with p-values of < 0.05 considered significant.

Supplementary Material

Refer to Web version on PubMed Central for supplementary material.

Acknowledgments

R.J.L. is an investigator with the Howard Hughes Medical Institute (HHMI). This work was supported in part by grants from the US National Institutes of Health to R.J.L. (HL16037) and to B.A.S. (R01HL65222). We gratefully acknowledge Drs. Brian Kobilka (Stanford University, Stanford, CA), and Georgios Skiniotis (University of Michigan, Ann Arbor, Michigan) for stimulating ideas and helpful discussions; we are also grateful to Drs. Sudarshan Rajagopal and Joshua C. Snyder of Duke University for discussions and critical reading of the manuscript; we thank Dr. Olivier Fedrigo, and Nicholas Hoang at the Genome Sequencing and Analysis Core Resource (Duke University) for library preparation support, quality control analysis, and performing Next-generations DNA sequencing; we also acknowledge the use of Transmission Electron Microscopy at the Shared Materials Instrumentation Facility (Duke university); T.J.C. is supported by the NHLBI grant of the National Institutes of Health (F30HL129803); we also thank Dr. Xin Chen (Changzhou University, Jiangsu, China) for the supply of BI167107; Drs. Arun K. Shukla (IIT, Kanpur, India), Elizabeth Pratico (Duke University), Jihee Kim (Duke University), and Kunhong Xiao (University of Pittsburg) for valuable assistance with reagents; Xinrong Jiang, and William Capel for excellent technical assistance; and Donna Addison and Quivetta Lennon for secretarial assistance.

REFERENCES

1. Pierce KL, Premont RT, Lefkowitz RJ. Seven-transmembrane receptors. Nat Rev Mol Cell Biol. 2002; 3:639–650. [PubMed: 12209124]
2. Lefkowitz RJ. A brief history of G-protein coupled receptors (Nobel Lecture). Angew Chem Int Ed Engl. 2013; 52:6366–6378. [PubMed: 23650015]
3. Lagerstrom MC, Schioth HB. Structural diversity of G protein-coupled receptors and significance for drug discovery. Nat Rev Drug Discov. 2008; 7:339–357. [PubMed: 18382464]
4. Kobilka BK. Amino and carboxyl terminal modifications to facilitate the production and purification of a G protein-coupled receptor. Anal Biochem. 1995; 231:269–271. [PubMed: 8678314]
5. Rajagopal S, Rajagopal K, Lefkowitz RJ. Teaching old receptors new tricks: biasing seven-transmembrane receptors. Nat Rev Drug Discov. 2010; 9:373–386. [PubMed: 20431569]
6. Violin JD, Crombie AL, Soergel DG, Lark MW. Biased ligands at G-protein-coupled receptors: promise and progress. Trends Pharmacol Sci. 2014; 35:308–316. [PubMed: 24878326]
7. Soergel DG, Subach RA, Cowan CL, Violin JD, Lark MW. First clinical experience with TRV027: pharmacokinetics and pharmacodynamics in healthy volunteers. J Clin Pharmacol. 2013; 53:892–899. [PubMed: 23813302]
8. Soergel DG, et al. Biased agonism of the mu-opioid receptor by TRV130 increases analgesia and reduces on-target adverse effects versus morphine: A randomized, double-blind, placebo-controlled, crossover study in healthy volunteers. Pain. 2014; 155:1829–1835. [PubMed: 24954166]
9. Kahsai AW, et al. Multiple ligand-specific conformations of the beta2-adrenergic receptor. Nat Chem Biol. 2011; 7:692–700. [PubMed: 21857662]
10. Liu JJ, Horst R, Katritch V, Stevens RC, Wuthrich K. Biased signaling pathways in beta2-adrenergic receptor characterized by 19F–NMR. Science. 2012; 335:1106–1110. [PubMed: 22267580]
11. Manglik A, et al. Structural Insights into the Dynamic Process of beta2-Adrenergic Receptor Signaling. Cell. 2015; 161:1101–1111. [PubMed: 25981665]
12. Rasmussen SG, et al. Structure of a nanobody-stabilized active state of the beta(2) adrenoceptor. Nature. 2011; 469:175–180. [PubMed: 21228869]
13. Rasmussen SG, et al. Crystal structure of the beta2 adrenergic receptor-Gs protein complex. Nature. 2011; 477:549–555. [PubMed: 21772288]
14. Granier S, Kobilka B. A new era of GPCR structural and chemical biology. Nat Chem Biol. 2012; 8:670–673. [PubMed: 22810761]
15. Ghosh E, Kumari P, Jaiman D, Shukla AK. Methodological advances: the unsung heroes of the GPCR structural revolution. Nat Rev Mol Cell Biol. 2015; 16:69–81. [PubMed: 25589408]
16. Kobilka B. The structural basis of G-protein-coupled receptor signaling (Nobel Lecture). Angew Chem Int Ed Engl. 2013; 52:6380–6388. [PubMed: 23650120]
17. Weichert D, et al. Covalent agonists for studying G protein-coupled receptor activation. Proceedings of the National Academy of Sciences of the United States of America. 2014; 111:10744–10748. [PubMed: 25006259]
18. Rosenbaum DM, et al. Structure and function of an irreversible agonist-beta(2) adrenoceptor complex. Nature. 2011; 469:236–240. [PubMed: 21228876]
19. Que-Gewirth NS, Sullenger BA. Gene therapy progress and prospects: RNA aptamers. Gene Ther. 2007; 14:283–291. [PubMed: 17279100]
20. Ng EW, et al. Pegaptanib, a targeted anti-VEGF aptamer for ocular vascular disease. Nat Rev Drug Discov. 2006; 5:123–132. [PubMed: 16518379]
21. Rusconi CP, et al. RNA aptamers as reversible antagonists of coagulation factor IXa. Nature. 2002; 419:90–94. [PubMed: 12214238]
22. Lincoff AM, et al. Effect of the REG1 anticoagulation system versus bivalirudin on outcomes after percutaneous coronary intervention (REGULATE-PCI): a randomised clinical trial. Lancet. 2016; 387:349–356. [PubMed: 26547100]
23. Ratner M. Next-generation AMD drugs to wed blockbusters. Nat Biotechnol. 2014; 32:701–702. [PubMed: 25101720]

24. Zhou J, et al. Cell-specific RNA aptamer against human CCR5 specifically targets HIV-1 susceptible cells and inhibits HIV-1 infectivity. Chem Biol. 2015; 22:379–390. [PubMed: 25754473]
25. Daniels DA, Sohal AK, Rees S, Grisshammer R. Generation of RNA aptamers to the G-protein-coupled receptor for neurotensin, NTS-1. Anal Biochem. 2002; 305:214–226. [PubMed: 12054450]
26. Lee G, et al. RNA based antagonist of NMDA receptors. ACS Chem Neurosci. 2014; 5:559–567. [PubMed: 24708087]
27. Pratico ED, Sullenger BA, Nair SK. Identification and characterization of an agonistic aptamer against the T cell costimulatory receptor, OX40. Nucleic Acid Ther. 2013; 23:35–43. [PubMed: 23113766]
28. Vinkenborg JL, Karnowski N, Famulok M. Aptamers for allosteric regulation. Nat Chem Biol. 2011; 7:519–527. [PubMed: 21769099]
29. Tesmer JJ. Crystallographic Pursuit of a Protein-RNA Aptamer Complex. Methods Mol Biol. 2016; 1380:151–160. [PubMed: 26552823]
30. Oberthur D, et al. Crystal structure of a mirror-image L-RNA aptamer (Spiegelmer) in complex with the natural L-protein target CCL2. Nat Commun. 2015; 6:6923. [PubMed: 25901662]
31. Tuerk C, Gold L. Systematic evolution of ligands by exponential enrichment: RNA ligands to bacteriophage T4 DNA polymerase. Science. 1990; 249:505–510. [PubMed: 2200121]
32. Ellington AD, Szostak JW. In vitro selection of RNA molecules that bind specific ligands. Nature. 1990; 346:818–822. [PubMed: 1697402]
33. Ozer A, Pagano JM, Lis JT. New Technologies Provide Quantum Changes in the Scale, Speed, and Success of SELEX Methods and Aptamer Characterization. Mol Ther Nucleic Acids. 2014; 3:e183. [PubMed: 25093707]
34. Shendure J, Ji H. Next-generation DNA sequencing. Nat Biotechnol. 2008; 26:1135–1145. [PubMed: 18846087]
35. Chae PS, et al. Maltose-neopentyl glycol (MNG) amphiphiles for solubilization, stabilization and crystallization of membrane proteins. Nat Methods. 2010; 7:1003–1008. [PubMed: 21037590]
36. Wang J, et al. Synthesis of β2-AR agonist BI-167107. Chinese Journal of Organic Chemistry. 2013; 33:634–639.
37. Whorton MR, et al. A monomeric G protein-coupled receptor isolated in a high-density lipoprotein particle efficiently activates its G protein. Proceedings of the National Academy of Sciences of the United States of America. 2007; 104:7682–7687. [PubMed: 17452637]
38. Weiss DR, et al. Conformation guides molecular efficacy in docking screens of activated beta-2 adrenergic G protein coupled receptor. ACS chemical biology. 2013; 8:1018–1026. [PubMed: 23485065]
39. Wisler JW, et al. A unique mechanism of beta-blocker action: carvedilol stimulates beta-arrestin signaling. Proceedings of the National Academy of Sciences of the United States of America. 2007; 104:16657–16662. [PubMed: 17925438]
40. De Lean A, Stadel JM, Lefkowitz RJ. A ternary complex model explains the agonist-specific binding properties of the adenylate cyclase-coupled beta-adrenergic receptor. The Journal of biological chemistry. 1980; 255:7108–7117. [PubMed: 6248546]
41. Hoffman BB, Lefkowitz RJ. Adrenergic receptors in the heart. Annu Rev Physiol. 1982; 44:475–484. [PubMed: 6280590]
42. Staus DP, et al. Regulation of beta2-adrenergic receptor function by conformationally selective single-domain intrabodies. Mol Pharmacol. 2014; 85:472–481. [PubMed: 24319111]
43. Jiang J, et al. The architecture of Tetrahymena telomerase holoenzyme. Nature. 2013; 496:187–192. [PubMed: 23552895]
44. Peisley A, Skiniotis G. 2D Projection Analysis of GPCR Complexes by Negative Stain Electron Microscopy. Methods Mol Biol. 2015; 1335:29–38. [PubMed: 26260592]
45. Kahsai AW, Rajagopal S, Sun J, Xiao K. Monitoring protein conformational changes and dynamics using stable-isotope labeling and mass spectrometry. Nat Protoc. 2014; 9:1301–1319. [PubMed: 24810039]

46. Steyaert J, Kobilka BK. Nanobody stabilization of G protein-coupled receptor conformational states. Curr Opin Struct Biol. 2011; 21:567–572. [PubMed: 21782416]

47. Hino T, et al. G-protein-coupled receptor inactivation by an allosteric inverse-agonist antibody. Nature. 2012; 482:237–240. [PubMed: 22286059]

48. Adams JJ, Sidhu SS. Synthetic antibody technologies. Curr Opin Struct Biol. 2014; 24:1–9. [PubMed: 24721448]

49. Ivetac A, McCammon JA. Mapping the druggable allosteric space of G-protein coupled receptors: a fragment-based molecular dynamics approach. Chem Biol Drug Des. 2010; 76:201–217. [PubMed: 20626410]

50. Wootten D, Christopoulos A, Sexton PM. Emerging paradigms in GPCR allostery: implications for drug discovery. Nat Rev Drug Discov. 2013; 12:630–644. [PubMed: 23903222]

REFERENCES (ONLINE METHODS only)

51. Denisov IG, Grinkova YV, Lazarides AA, Sligar SG. Directed self-assembly of monodisperse phospholipid bilayer Nanodiscs with controlled size. J Am Chem Soc. 2004; 126:3477–3487. [PubMed: 15025475]

52. Bompiani KM, Monroe DM, Church FC, Sullenger BA. A high affinity, antidote-controllable prothrombin and thrombin-binding RNA aptamer inhibits thrombin generation and thrombin activity. J Thromb Haemost. 2012; 10:870–880. [PubMed: 22385910]

53. Shenoy SK, et al. beta-arrestin-dependent, G protein-independent ERK1/2 activation by the beta2 adrenergic receptor. The Journal of biological chemistry. 2006; 281:1261–1273. [PubMed: 16280323]

54. Williams RJ, Kelly E. Measurement of adenylyl cyclase activity in cell membranes. Methods Mol Biol. 1995; 41:63–77. [PubMed: 7655568]

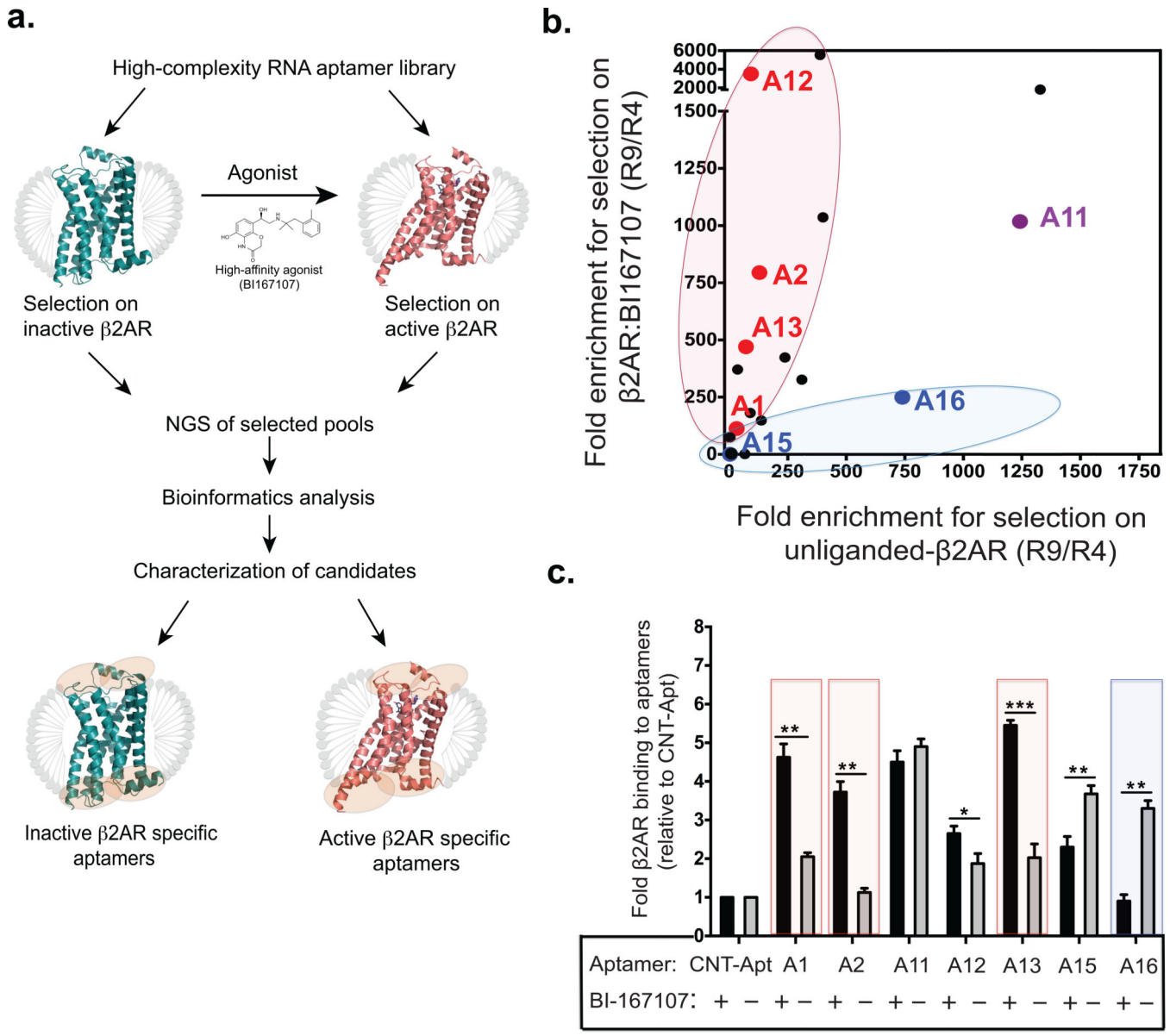

Figure 1. Generation of conformation-specific RNA aptamers against the β_2AR

(**a**) Schematic overview of the selection strategy, NGS, bioinformatics analysis, and characterization of candidate aptamers. Ribbon diagram representation for selection against inactive β_2AR (colored in blue; PDB: 2RH1) or active β_2AR bound to high affinity agonist BI167107 (colored in red; PDB: 3SN6). MNG detergent micelles are represented in gray. Encircled orange areas show potential binding regions for aptamers to different β_2AR conformations. (**b**) Scatter plot from NGS analysis, comparing fold enrichment-ratios (R4 to R9) for the top 20-aptamer sequences from selection on unliganded β_2AR (*x*-axis) *versus* BI167107-bound β_2AR (*y*-axis). Each point in the plot represents a unique aptamer (the top seven candidate binders are color-coded in red, blue, or purple) according to their enrichment and selectivity to a selection target. (**c**) Bar graph shows top seven aptamers and their capacity to bind unliganded β_2AR or BI167107-bound β_2AR as assessed by pull-down

assay. Boxed bars denote the four aptamers, selected for further characterization. Data shown represent the mean ± s.e.m. (*$P < 0.05$; **$P < 0.01$; ***$P < 0.001$) of three independent experiments, analyzed by one-way ANOVA followed by a Fisher's LSD post-test.

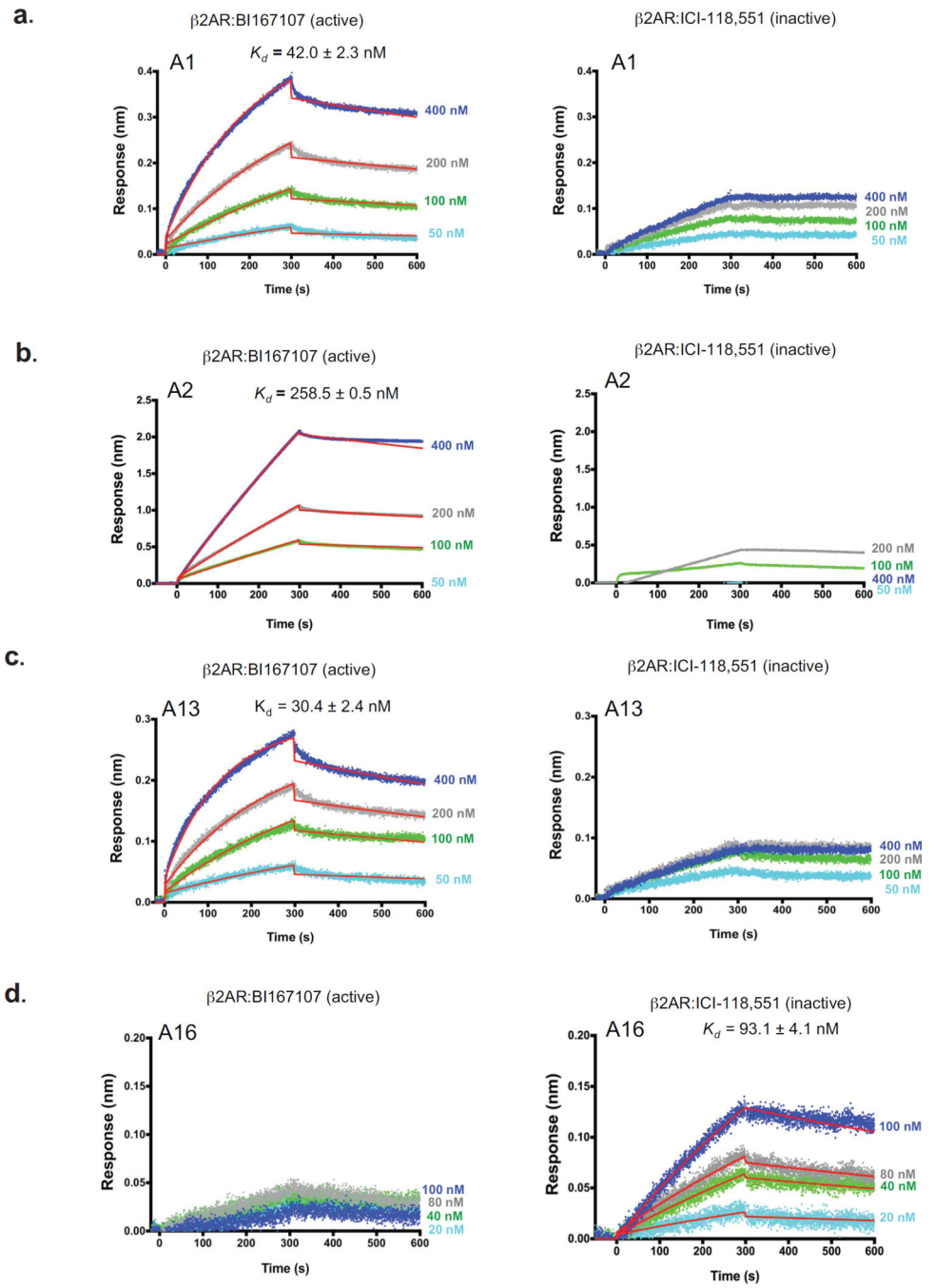

Figure 2. Aptamers distinguish between inactive and active conformations of the β_2AR

Binding kinetic profiles for the interactions of four biotinylated aptamers with BI167107-bound (active) β_2AR or ICI-118,551-bound (inactive) β_2AR as analyzed using biolayer interferometry (BLI). (**a–d**) Representative sensorgrams for the interactions of four biotinylated aptamers with BI167107-bound β_2AR (left panels) or ICI-118,551-bound β_2AR (right panels): A1 (**a**), A2 (**b**), A13 (**c**), and A16 (**d**). Data was globally fit to 1:1 binding model as described in methods. K_d (dissociation constant) is shown as the ratio of k_{off} (dissociation) to k_{on} (association) rate constants. Each K_d value represents the mean affinity

values ± s.e.m. of three independent experiments. Blue, gray, green, and light blue curves represent the measured responses for each tested concentration of β_2AR (BI167107 or ICI-118,551-bound β_2AR). Whereas overlay the curves in red show the global fitting results of the binding data.

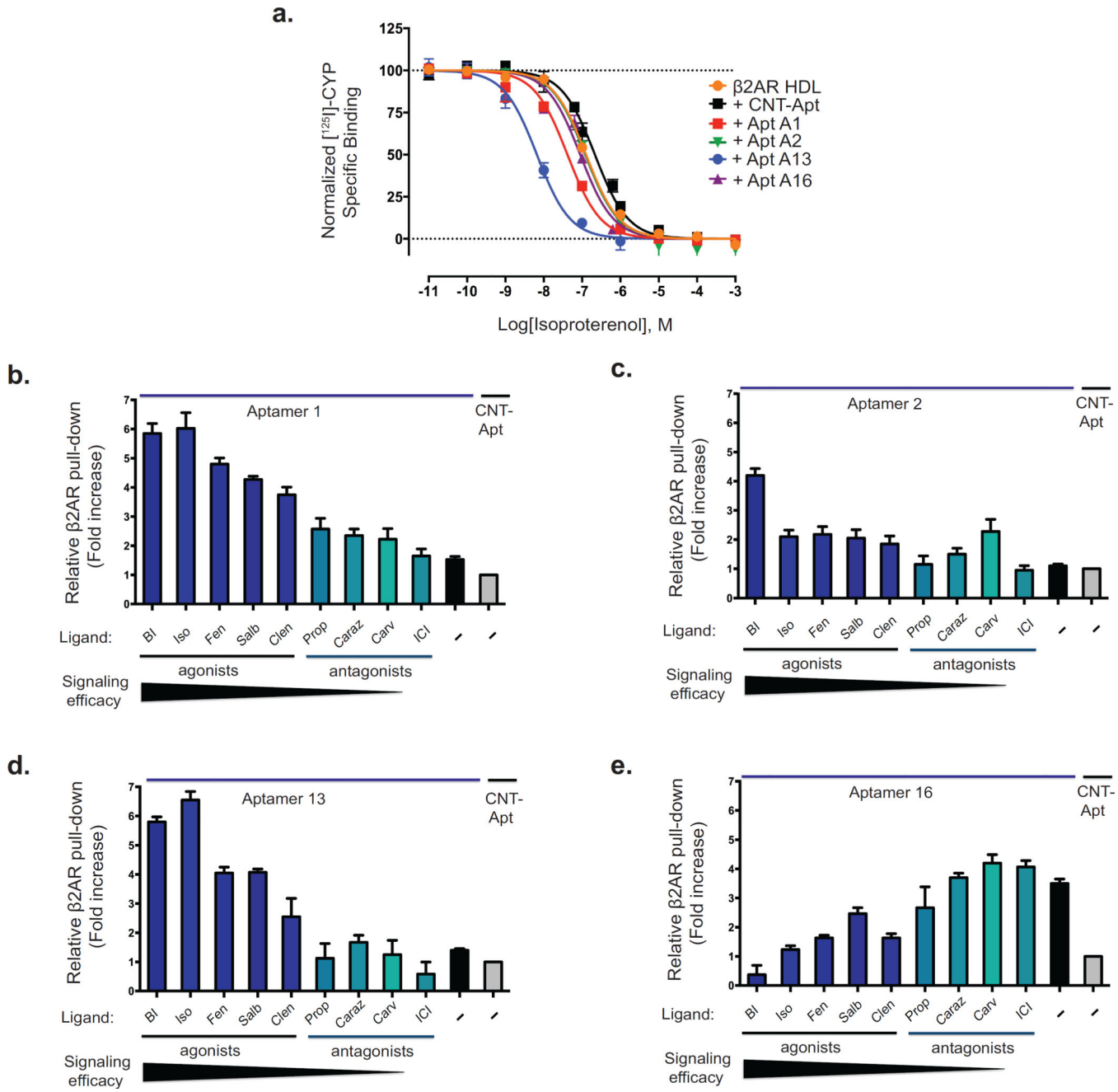

Figure 3. Selectivity of aptamers for specific β_2AR conformations correlates with receptor ligand efficacy or ligand specificity

(a) Dose-response curves for the competition of the radioiodinated antagonist cyanopindolol ([^{125}I]-CYP) binding with isoproterenol in β_2AR reconstituted within HDL particles in the presence or absence of aptamers (A1, A2, A13, A16 or CNT-Apt). The ordinates represent the specific binding of 60 pmol/L [^{125}I]-CYP in the presence of different concentrations of ISO. Curves were obtained from three independent experiments. Error bars represent standard errors. **(b–e)** Western blotting analyses from binding experiments using specified biotinylated aptamers (A1, A2, A13 or A16) interacting with β_2AR in the absence or

presence of various ligands. Agonists are shown (bars, royal blue) and antagonists (bars, cyan). Structures and functional properties of the nine β-adrenoceptor ligands are shown in Supplementary Figure 6. Binding of four aptamers to various forms of β_2AR: A1 (**b**) and A13 (**d**) preference for agonist-bound β_2AR; A2 (**c**) preference for ligand-specific form of β_2AR; and A16 (**e**) preference for antagonist-bound β_2AR. Aptamer input is indicated by ethidium bromide staining of the eluted RNA. Data correspond to the mean ± standard error of at least three independent experiments.

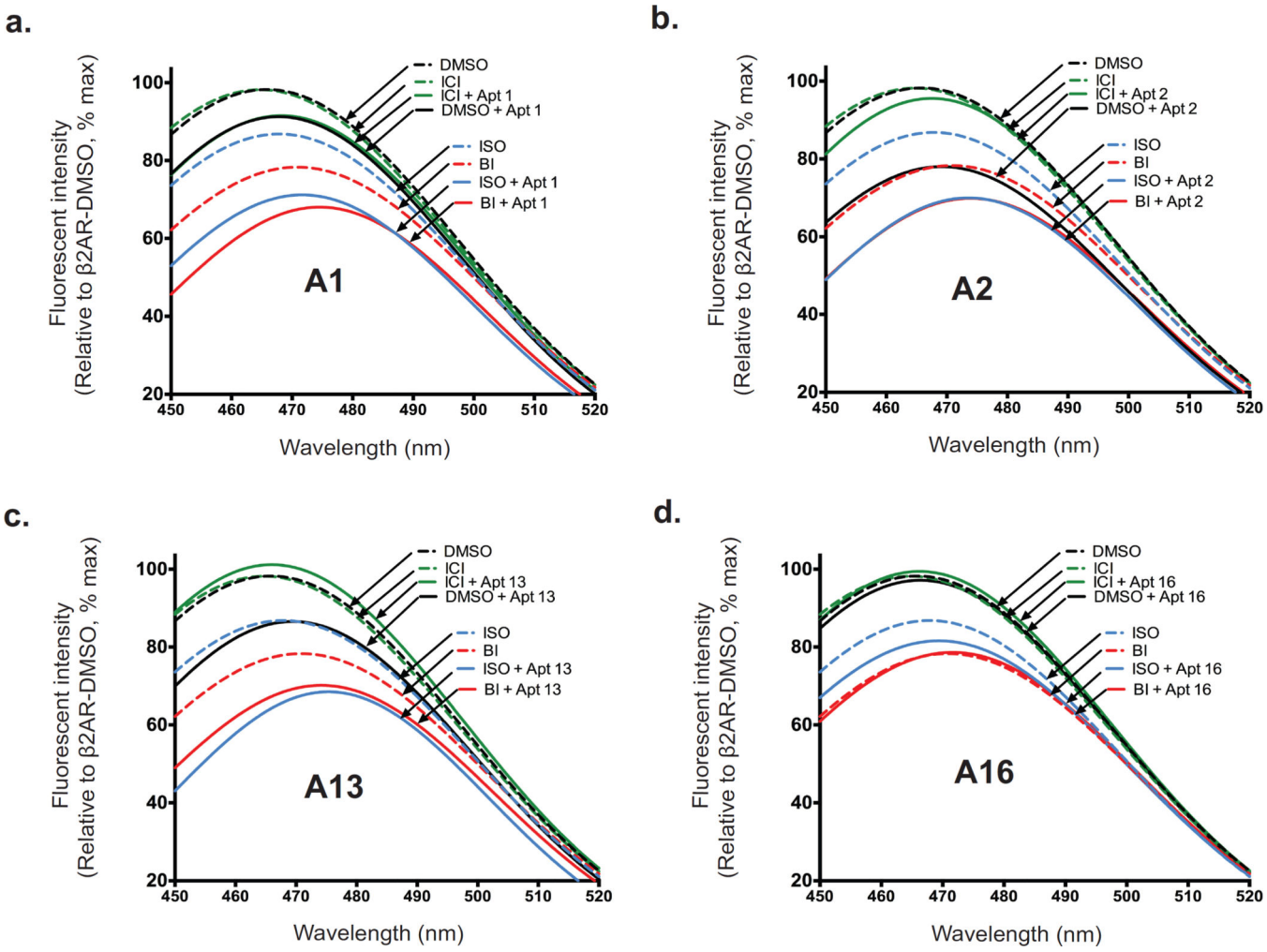

Figure 4. Influence of aptamers on conformational changes conferred by ligands

(**a–d**) Bimane fluorescence quenching measurement shows that aptamers A1, A2, and A13 stabilize active forms of β_2AR, while aptamer A16 stabilizes an inactive conformation. Bimane fluorescence quenching measurement detects conformational changes of the β_2AR via movement of a bimane probe on TM6 (at C265) upon the binding of agonists, (BI167107 [BI] or isoproterenol [ISO]) and/or aptamer: A1 (**a**), A2 (**b**), A13 (**c**) or A16 (**d**). Fluorescence emission spectra showing ligand-induced conformational changes of bimane-labeled β_2AR in the absence (black dashed line) or presence of full agonist (ISO, blue dashed line, or BI, red dashed line), inverse agonist ICI-118,551 (ICI, green dashed line), aptamer A1, A2, A13, or A16 (black solid line), or a combination of aptamer (A1, A2, A13, or A16) with ISO (blue solid line), BI (red solid line), or ICI (green solid line).

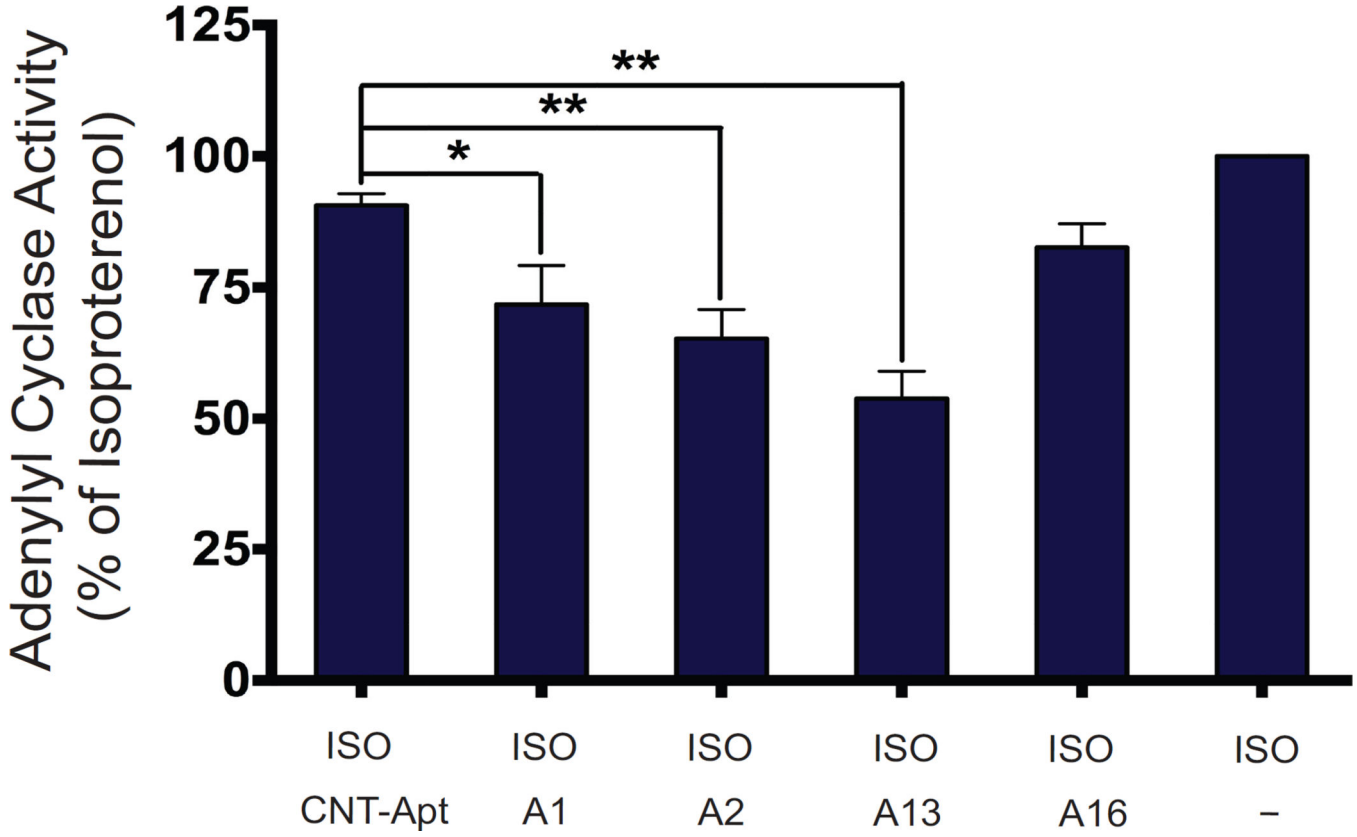

Figure 5. Functional effect of aptamers on β_2AR–mediated Gα_s and AC activation

β_2AR-dependent stimulation of AC activity and accumulation of cAMP was measured in HEK-293 membrane homogenates stably expressing β_2AR (expression level: ~2.5 pmoles/mg) in the presence of 100 nM of isoproterenol (ISO) or combination of 100 nM ISO with aptamer (A1, A2, A13, A16 or control aptamer). Data represents the means ± s.e.m. of at least four independent experiments. Asterisks in the bar graphs denote significant differences (*$P < 0.05$; **$P < 0.01$) by one-way ANOVA (with Tukey's multiple comparisons test) from results for AC activity performed with control aptamer.

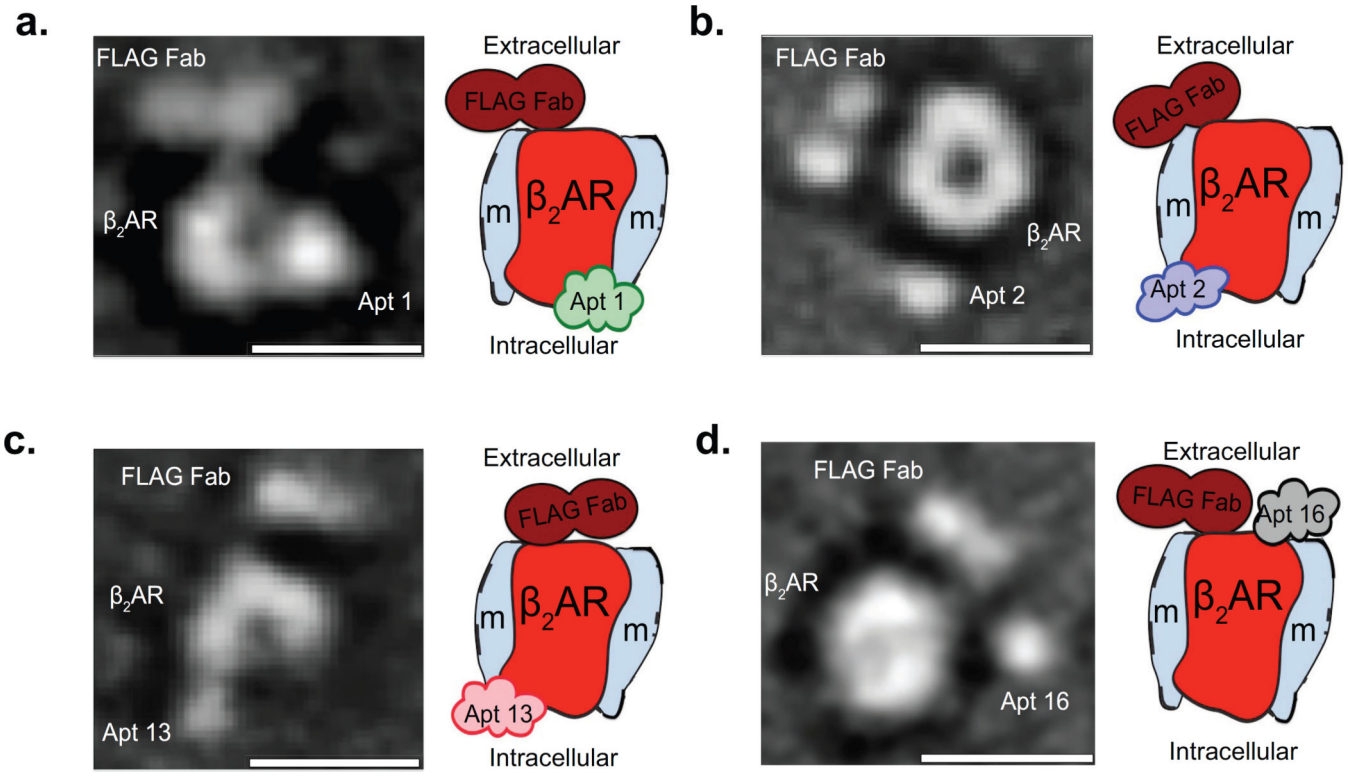

Figure 6. EM analysis and molecular architecture of β_2AR–aptamer complexes

(**a–d**) EM characterization of purified β_2AR-aptamer-Fab complexes. Shown on the left side of each panel are two-dimensional (2D) particle class average particles of the β_2AR–aptamer-Fab complexes. Scale bar is 10 nm. The left side of each panel shows 2D particle averages of anti-FLAG Fab labeled β_2AR in complex with aptamer A1 (**a**), A2 (**b**), A13 (**c**) or A16 (**d**). The right side of each panel shows a cartoon representation of the class average; the various components in the 2D–image maps (β_2AR in red; detergent micelle labeled with "m" in light-gray; anti-FLAG Fab antibody in dark-red; the aptamers in lime-green [A1], medium-purple [A2], pink [A13] and gray [A16]).